Electronic Supplementary Material (ESI) for Dalton Transactions.

Supporting Information

Subphthalocyanines as fluorescence sensors for metal cations

Mary Angelia Alfred,[a] Kamil Lang,[b] Kaplan Kirakci,[b] Pavel Stuzhin,[c] Petr Zimcik[a], Jan Labuta, *[d] and Veronika Novakova*[a]

[a] Faculty of Pharmacy in Hradec Kralove, Charles University, Ak. Heyrovskeho 1203, Hradec Kralove, 500 05 Czech Republic.
[b] Institute of Inorganic Chemistry of the Czech Academy of Sciences, 250 68 Husinec-Řez, Czech Republic.
[c] Institute of Macroheterocycles, Ivanovo State University of Chemistry and Technology, Sheremetevskij Pr-t 7, 153000 Ivanovo, Russia
[d] Research Center for Materials Nanoarchitectonics (MANA), National Institute for Materials Science (NIMS), 1-1 Namiki, Tsukuba, Ibaraki 305-0044, Japan

Content

NMR spectra

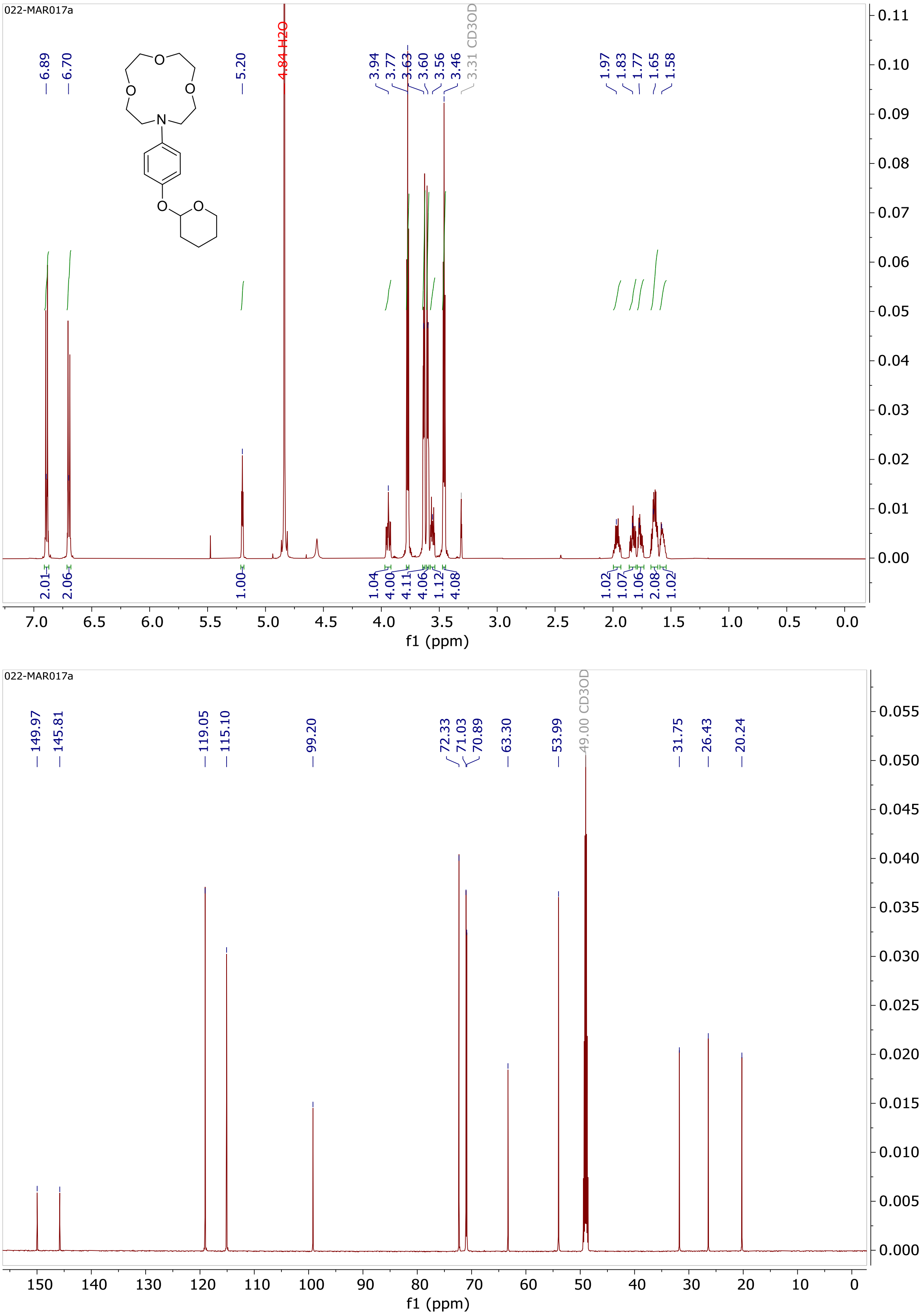

Fig. S1. ^{1}H NMR (600 MHz, Methanol-d_4) and ^{13}C NMR (151 MHz, Methanol-d_4) spectra of compound **2a**.

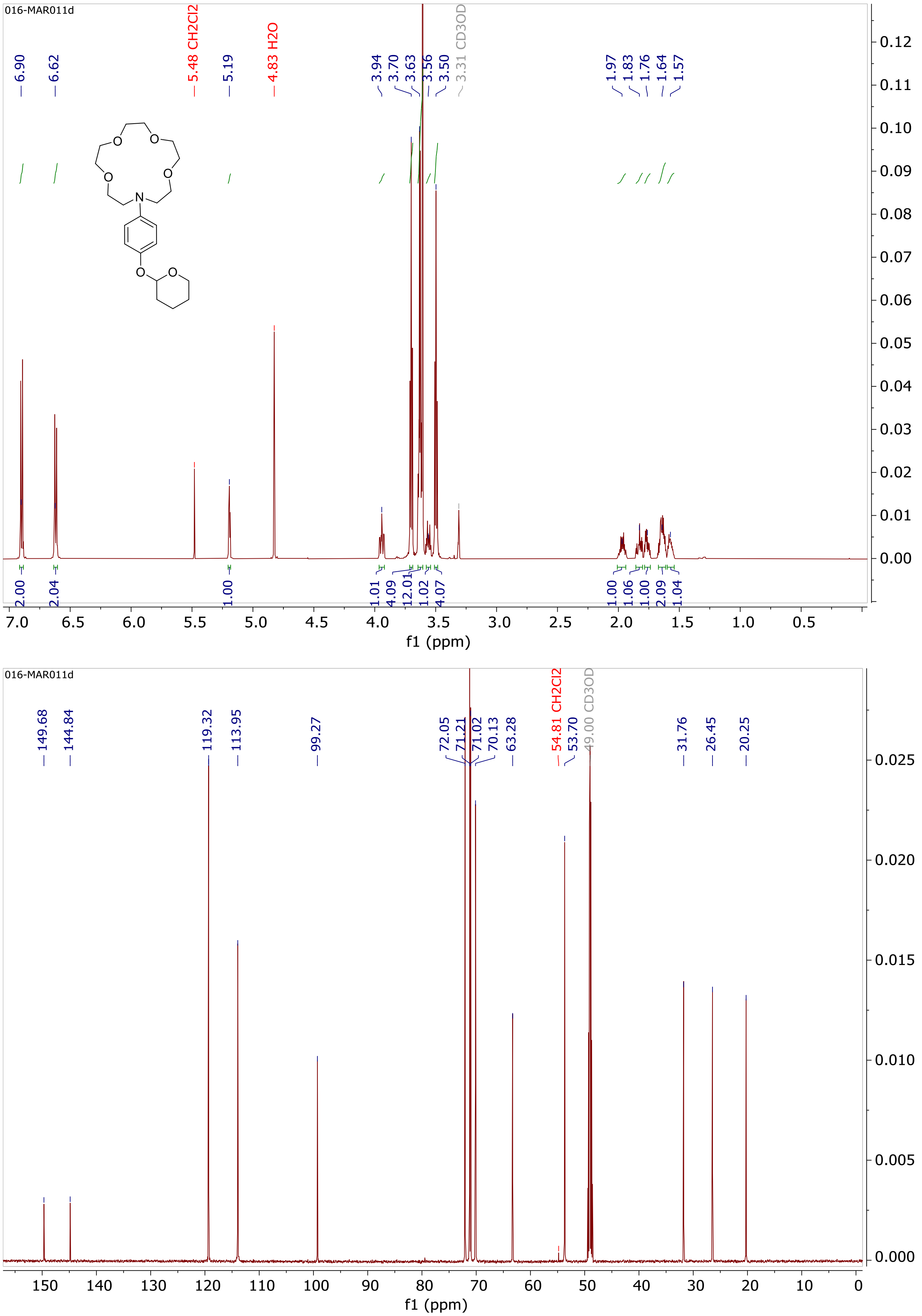

Fig. S2. ^{1}H NMR (600 MHz, Methanol-d_4) and ^{13}C NMR (151 MHz, Methanol-d_4) spectra of compound **2b**.

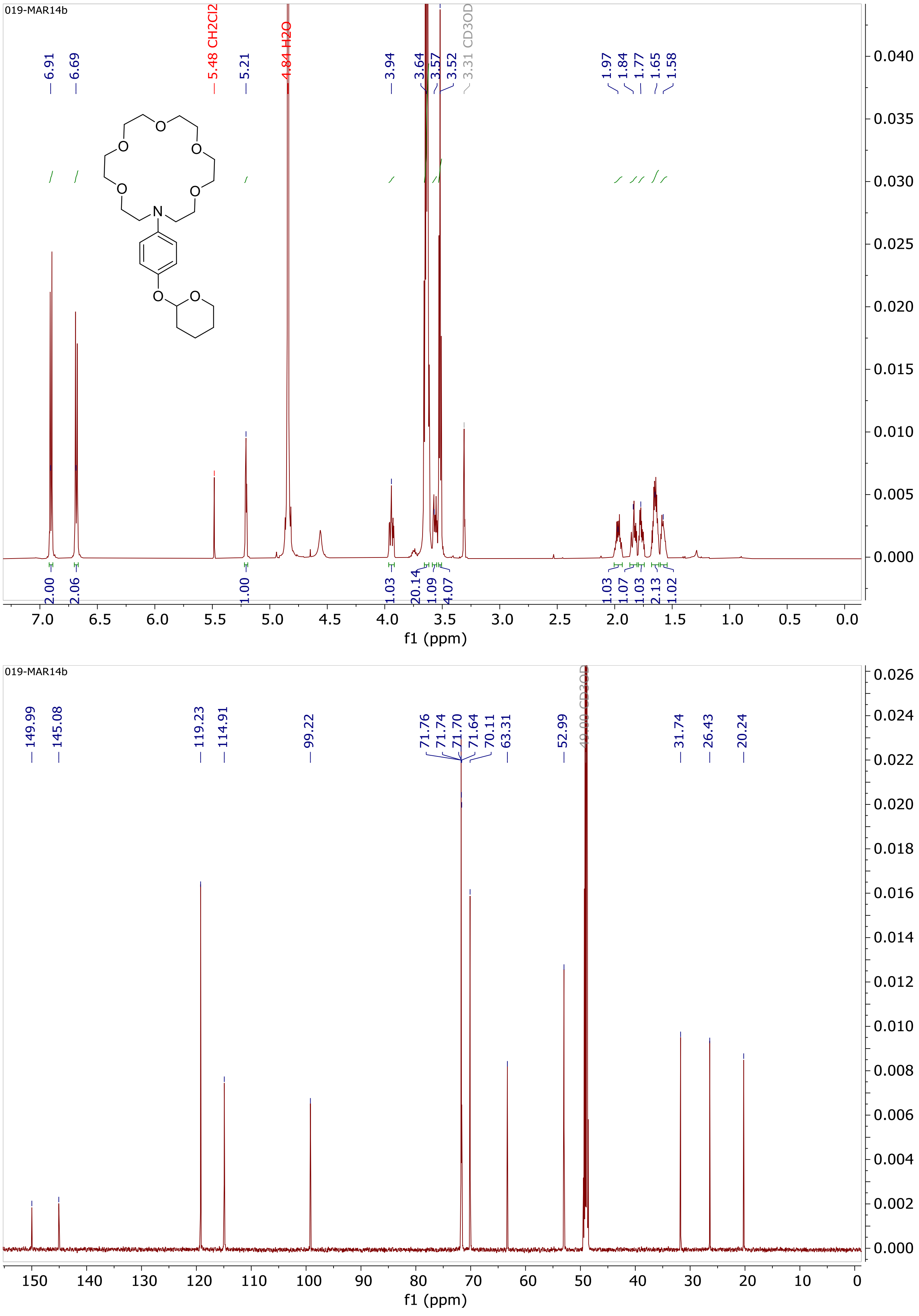

Fig. S3. ^{1}H NMR (600 MHz, Methanol-*d*$_4$) and ^{13}C NMR (151 MHz, Methanol-*d*$_4$) spectra of compound **2c**.

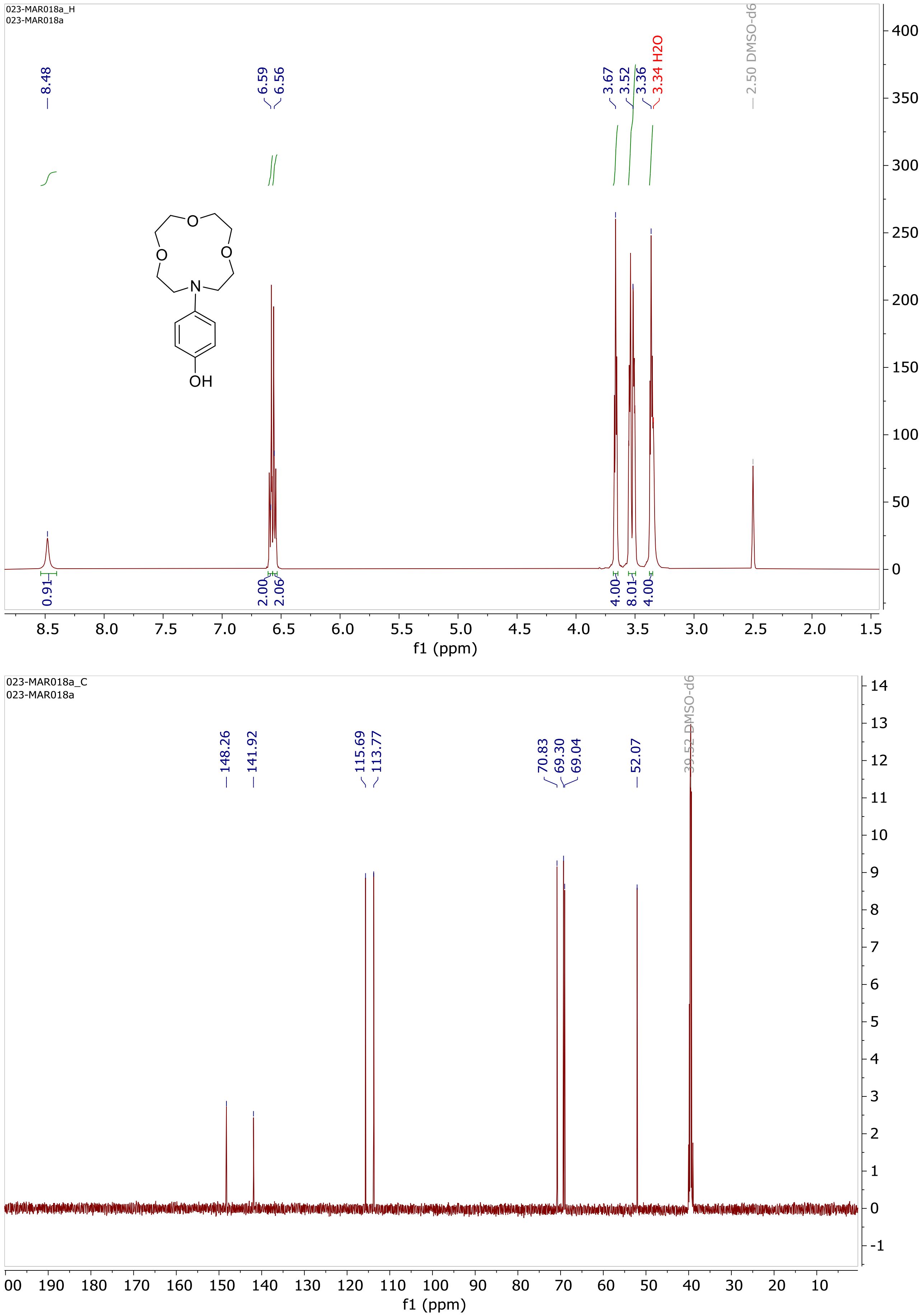

Fig. S4. ^{1}H NMR (500 MHz, DMSO-d_6) and ^{13}C NMR (126 MHz, DMSO-d_6) spectra of **3a**.

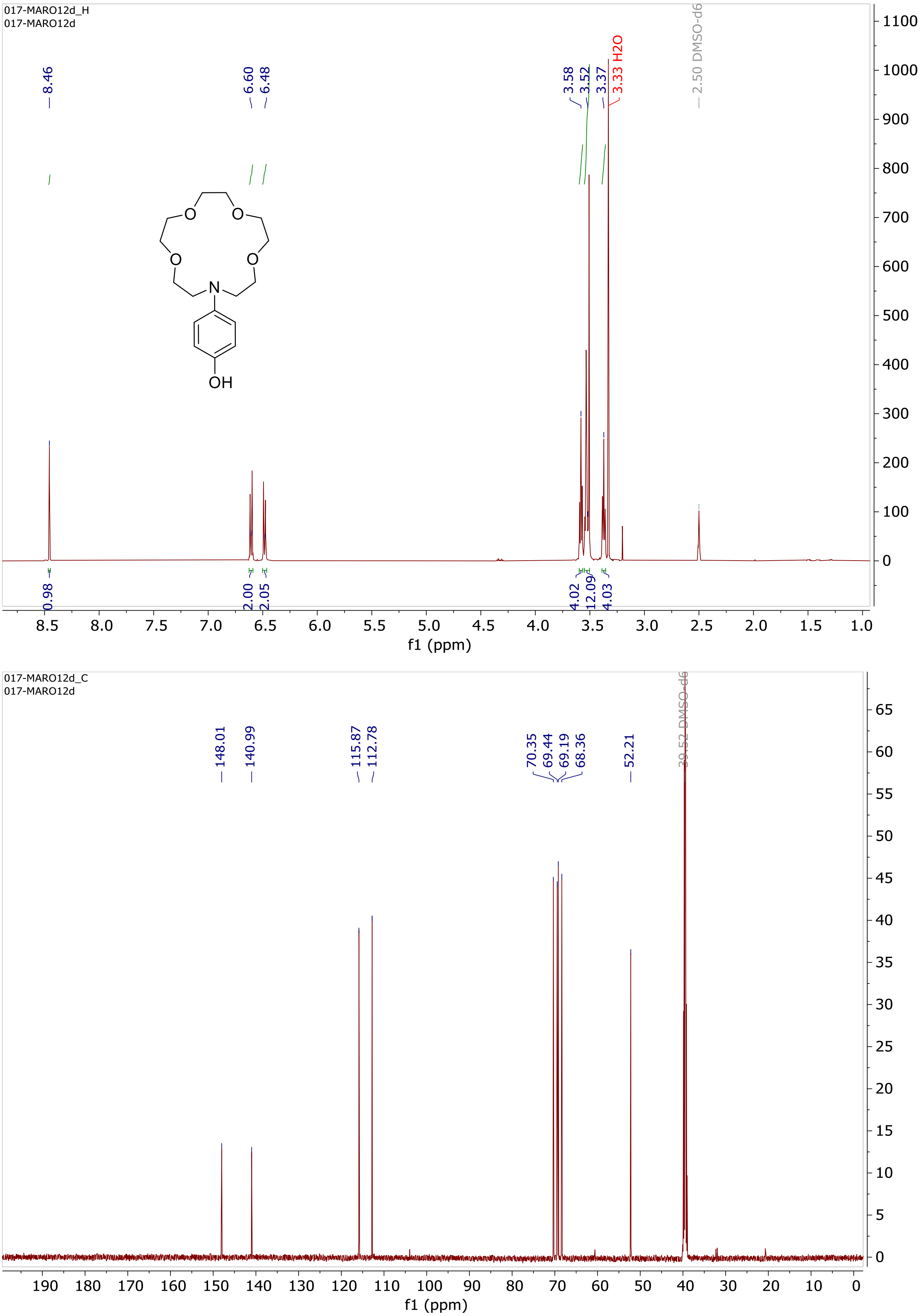

Fig. S5. ^{1}H NMR (500 MHz, DMSO-d_6) and ^{13}C NMR (126 MHz, DMSO-d_6) spectra of compound **3b**.

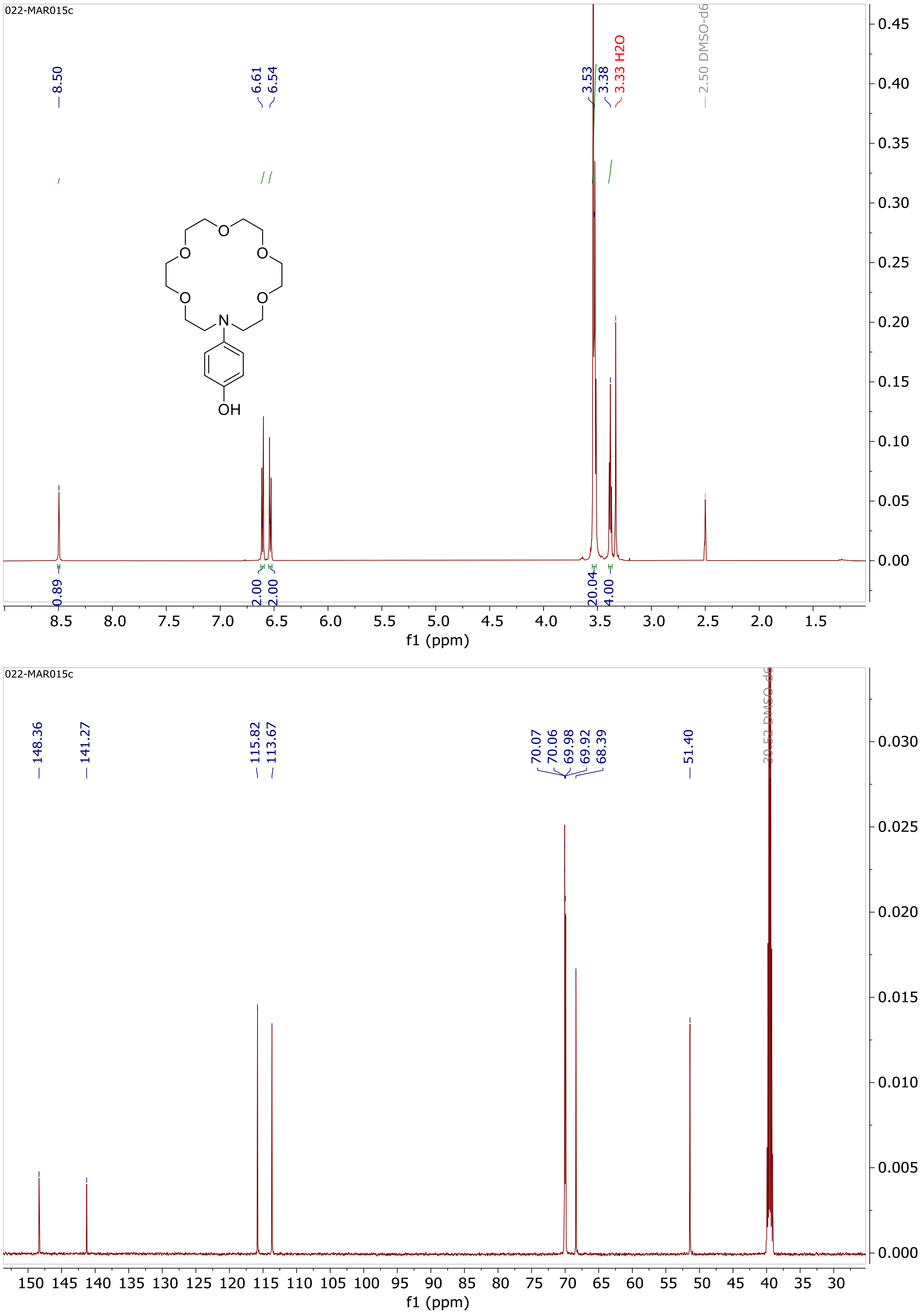

Fig. S6. ^{1}H NMR (600 MHz, DMSO-*d*$_6$) and ^{13}C NMR (151 MHz, DMSO-*d*$_6$) spectra of compound **3c**.

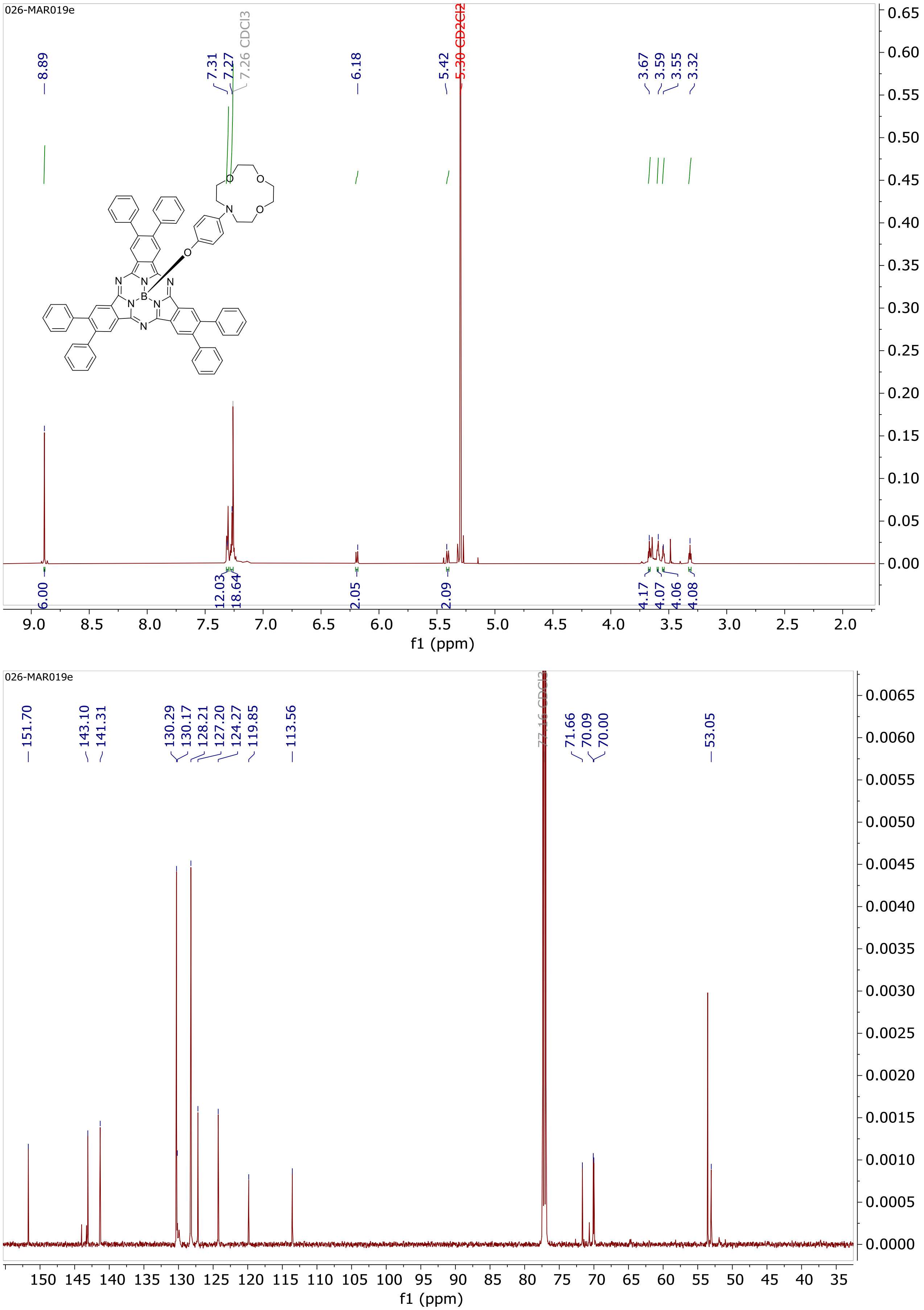

Fig. S7. ^{1}H NMR (600 MHz, CDCl$_3$) and ^{13}C NMR (151 MHz, CDCl$_3$) spectra of compound **6a.**

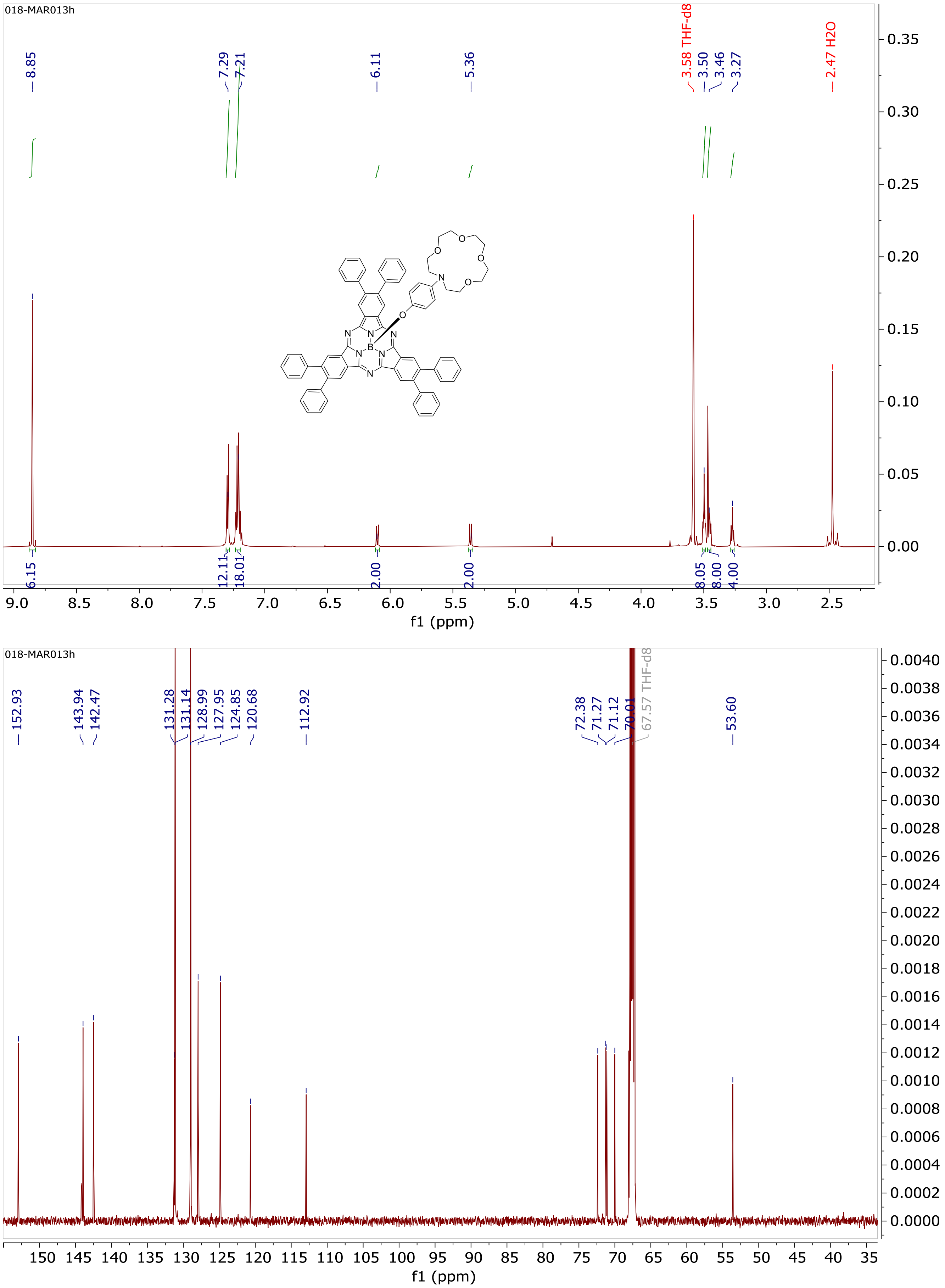

Fig. S8. ^{1}H NMR (600 MHz, THF-d_8) and ^{13}C NMR (151 MHz, THF-d_8) spectra of compound **6b.**

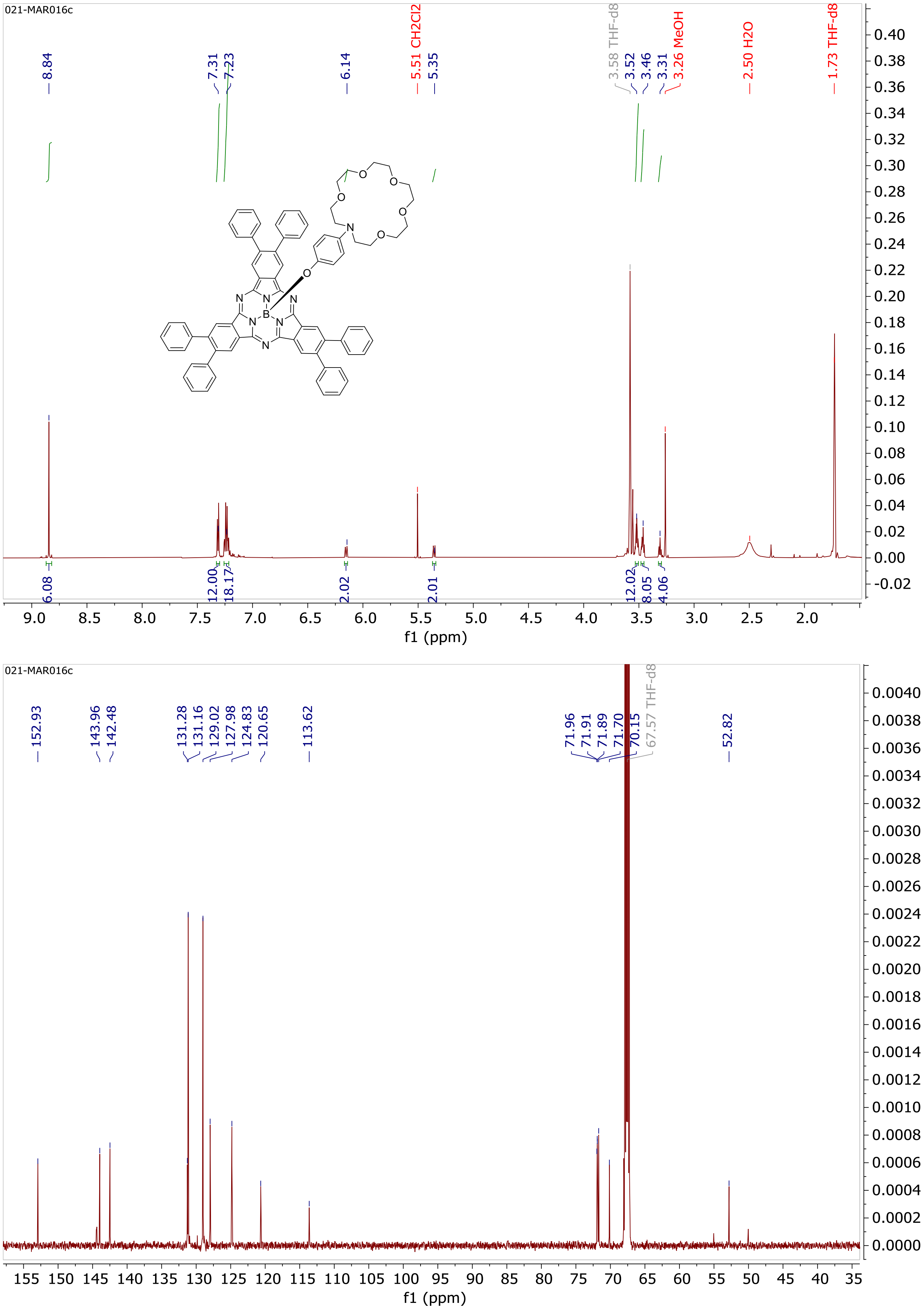

Fig. S9. ^{1}H NMR (600 MHz, THF-d_8) and ^{13}C NMR (151 MHz, THF-d_8) Spectra of compound **6c**.

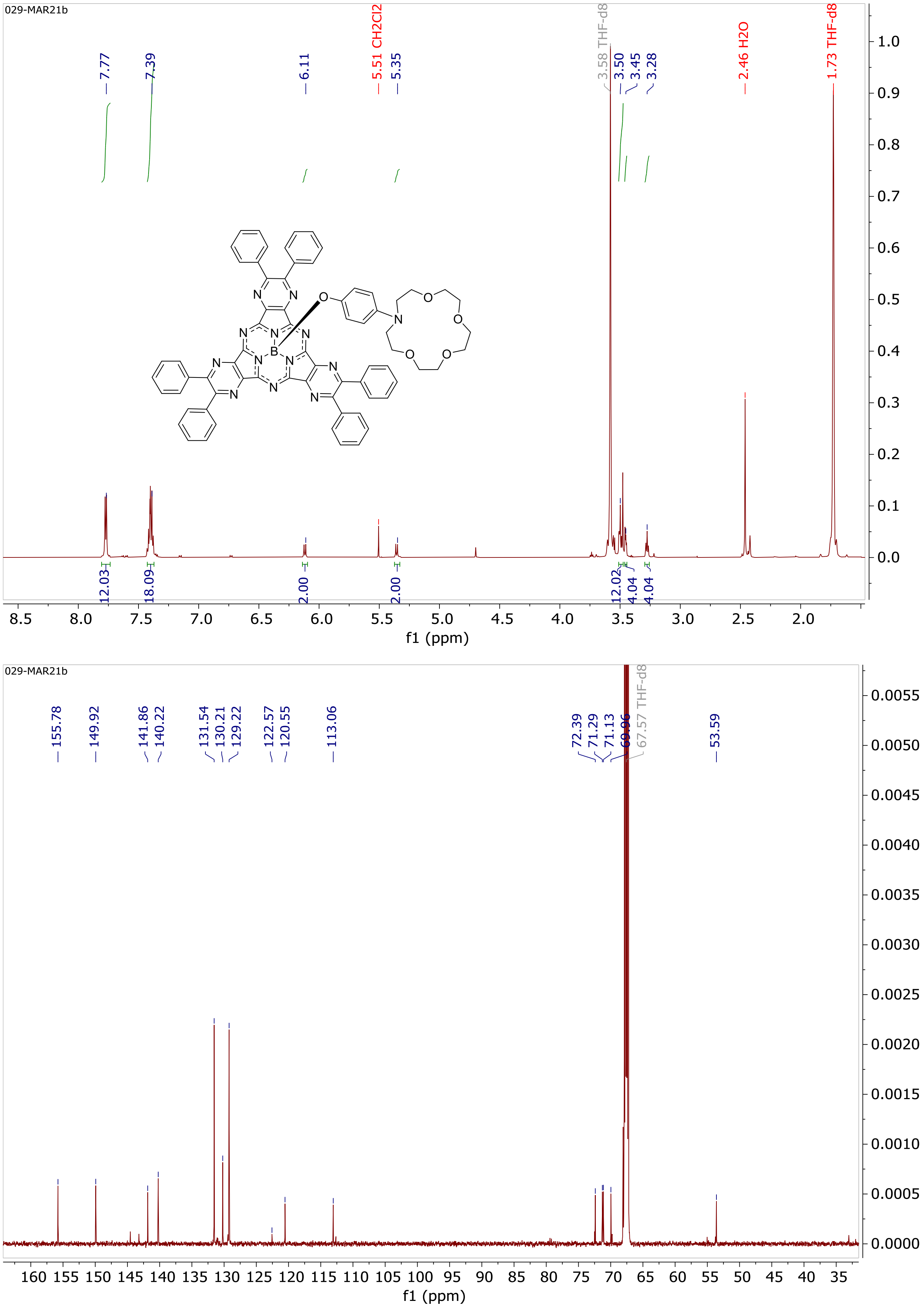

Fig. S10. ^{1}H NMR (600 MHz, THF-d_8) and ^{13}C NMR (151 MHz, THF-d_8) Spectra of compound **7b**.

Decomposition studies

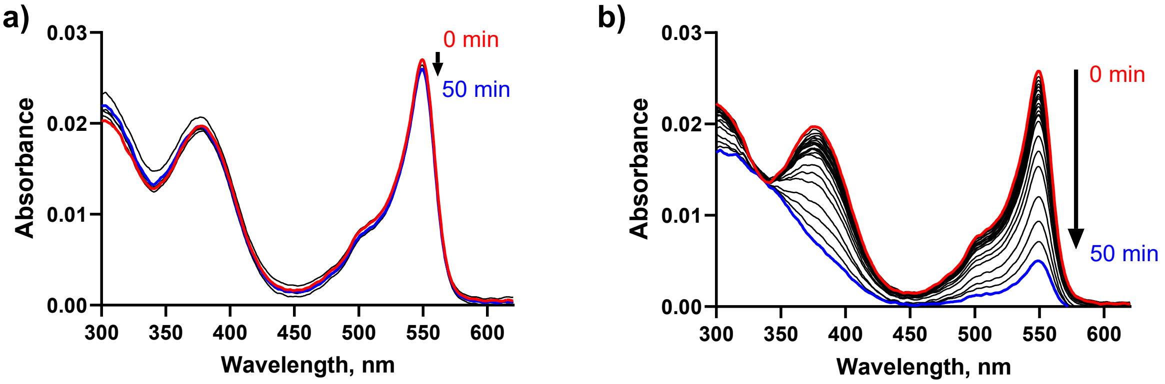

Fig. S11. Changes in absorption spectra of **7b** (1 µM, THF) in dark (a) and after light iradiation (b) (100W Xe-ozone free lamp, Newport).

Effect of counter-anion

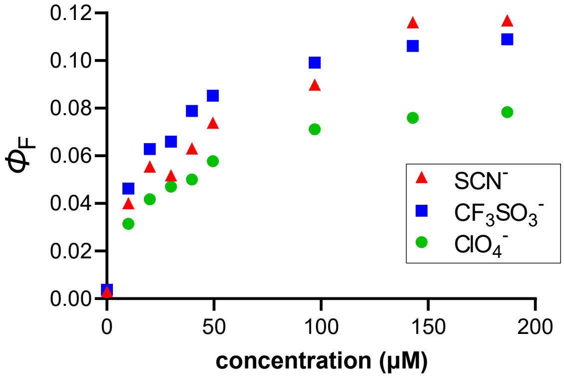

Fig. S12. Increase in Φ_F of **6c** (1µM in THF) as a model compound upon addition of different potassium salts (KSCN, KCF_3SO_3 and $KClO_4$; stock solutions in MeOH). λ_{exc} = 505 nm.

Stoichiometry studies by ^{1}H NMR titrations

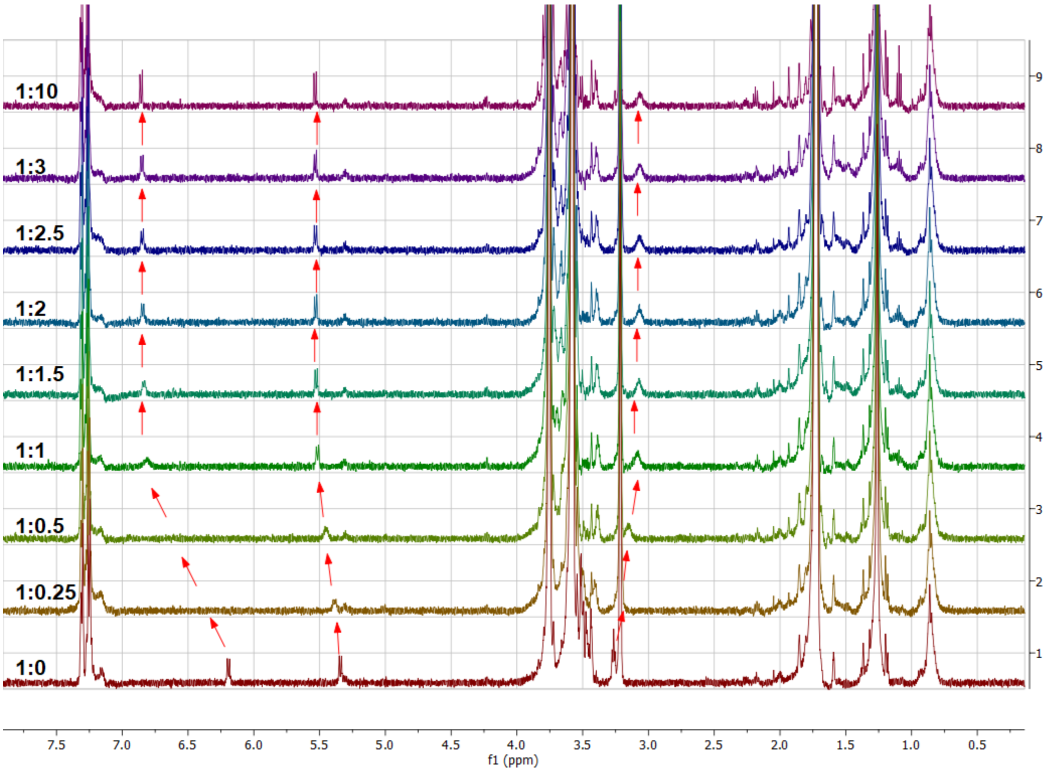

Fig. S13. ^{1}H NMR spectra (600 MHz, THF-d_8/MeOH-d_4 5:2) of **6c** with Ba(OTf)$_2$ at different compound:salt ratios. The resonance at 6.2 ppm broadens in the initial phase of titration due to the intermediate exchange rate.

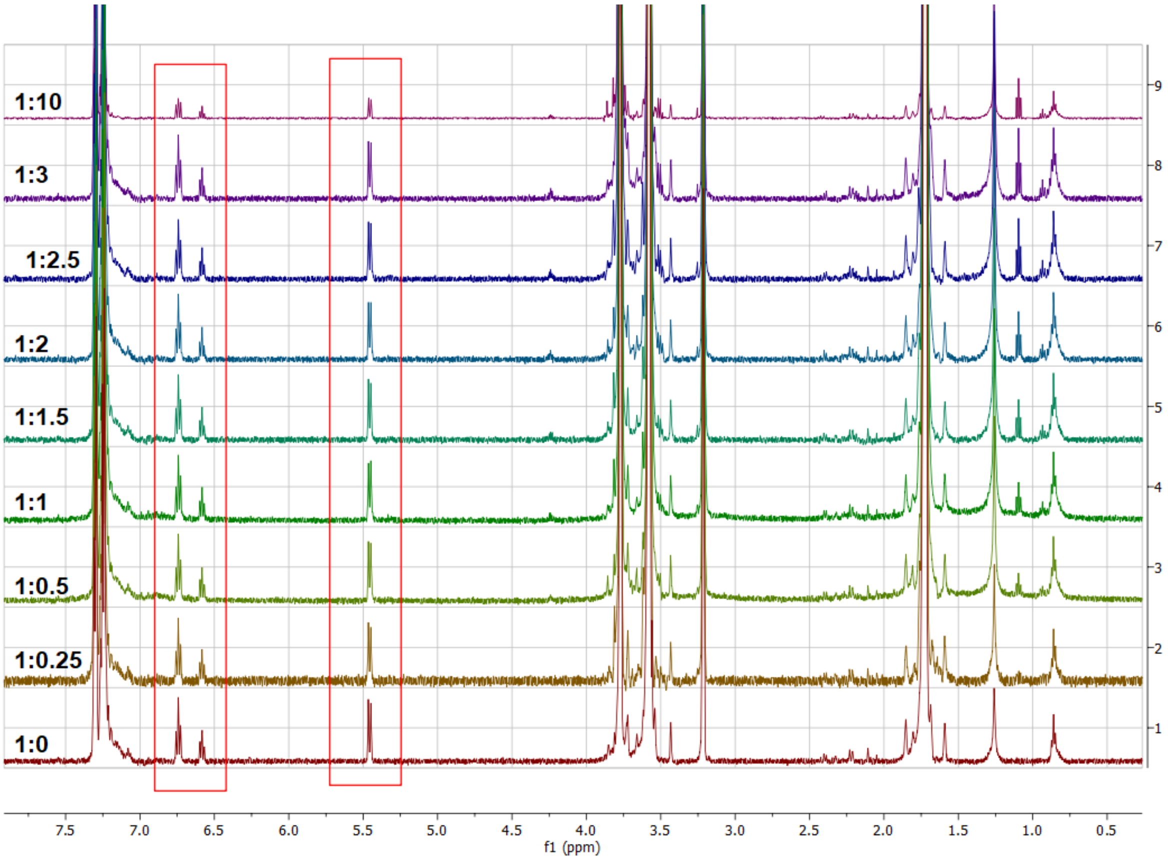

Fig. S14. ^{1}H NMR spectra (600 MHz, THF-d_8/MeOH-d_4 5:2) of control compound **6d** with KOTf at different compound:salt ratios.

Stoichiometry studies by Job´s method of continuous variation

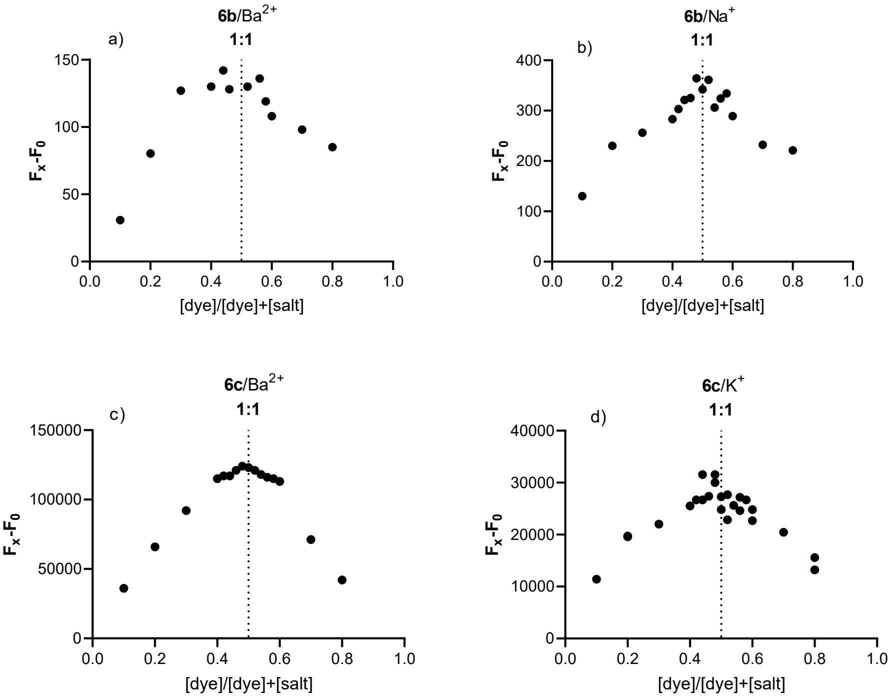

Fig. S15. Assessment of stoichiometry of binding for **6b** (a,b) and **6c** (c,d) with the sensitive cations by observation of changes in fluorescence emission before (F_0) and after the addition of analyte (F_x). For the procedure, see the Experimental part in the main manuscript.

Summary of obtained apparent binding constants K_a

Table S1. Apparent binding constants K_a [a] and colour coding based on fluorescence enhancement factor (FEF)[b].

Method	Compound	Axial ligand	Li^+	Na^+	K^+	Ca^{2+}	Mg^{2+}	Ba^{2+}
Fluorescence	**6a**	1-aza-4-crown-12	9.9	0	0	500	9080	192000
Fluorescence	**6b**	1-aza-5-crown-15	5.5	615	76	58	520	12800
Fluorescence	**6c**	1-aza-6-crown-18	5.7	1940	36100	11300	6200	384000
NMR [c]	**6c**	1-aza-6-crown-18	N/D	N/D	34800	N/D	N/D	>230000

[a] All values have relative error <15%. [b] Small (≤ 15) and large FEF (≥ 40) (as shown in Table 1) are denoted by blue and red background, respectively. [c] Determined from axial phenyl linker resonances at 5.33 and 6.18 ppm.

Binding isotherms as obtained from fluorescence measurements

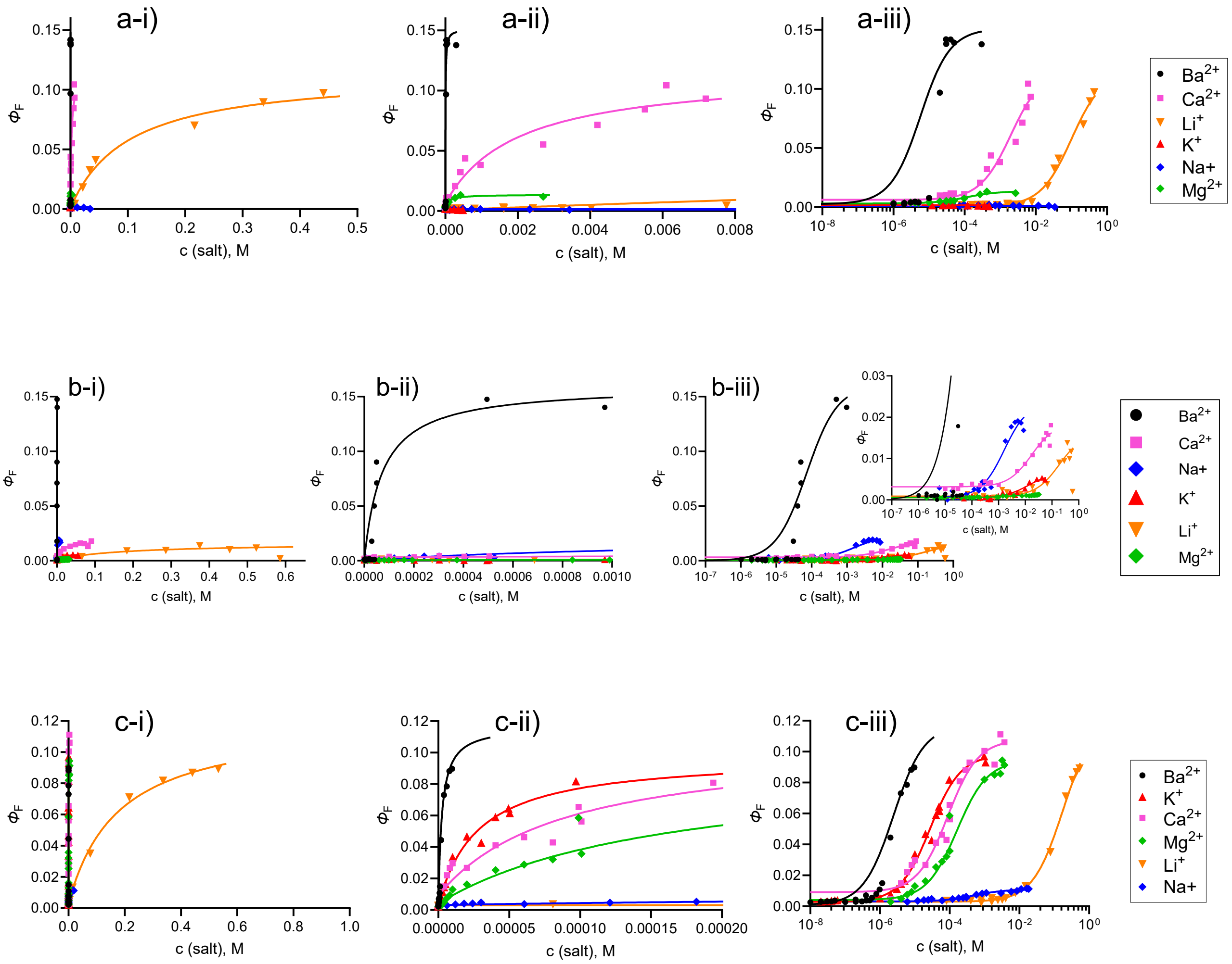

Fig. S16. Binding isotherms (Φ_F) at 25 °C upon addition of analyte (in the form of triflates) for hosts: (a) **6a**, (b) **6b** and (c) **6c**. The total concentration of hosts **6a**, **6b** and **6c** is 1 μM. Each set of isotherms is plotted in three scales (i) whole range, (ii) enlarged initial part and (iii) logarithmic scale. The lines are fitted isotherms based on 1:1 host-guest model.

Effects of water content on binding properties of **6c** with Ba^{2+} and K^+

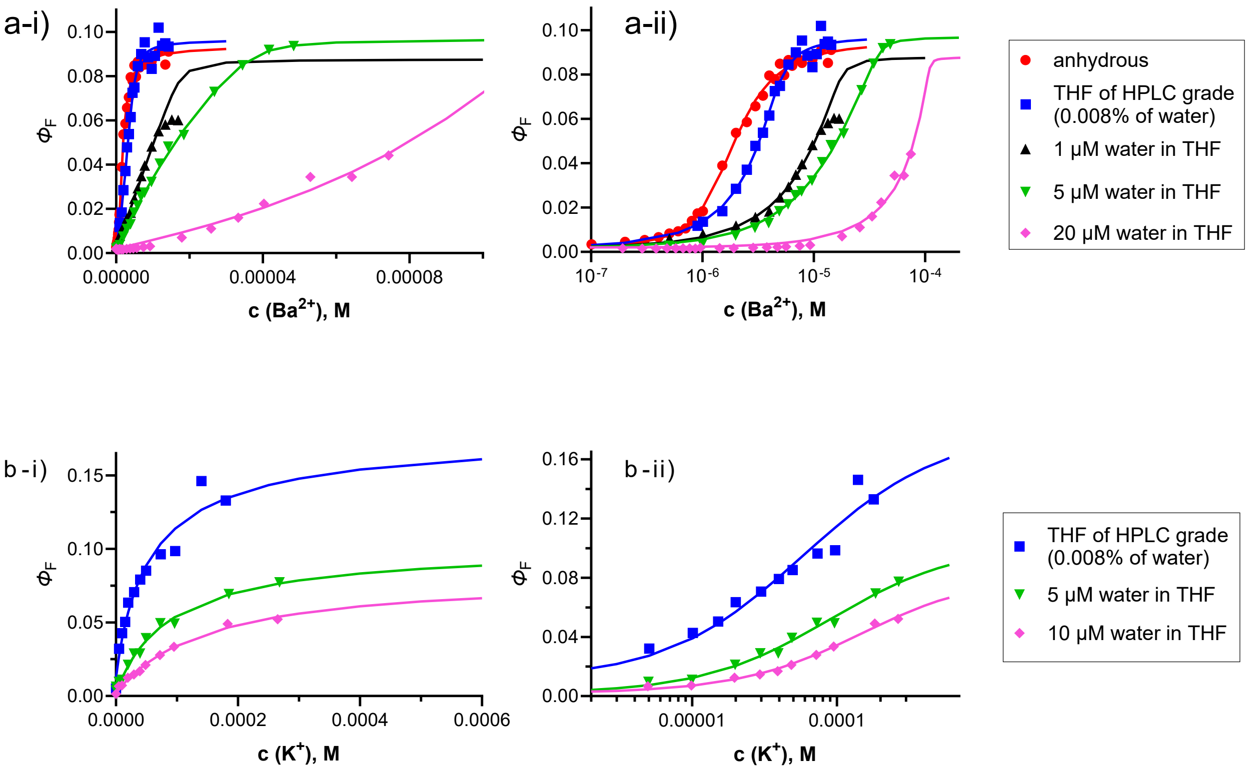

Fig. S17. Binding isotherms (Φ_F) at 25 °C upon addition of (a) Ba^{2+} and (b) K^+ cations (in the form of triflates) into the solution of **6c** (1 µM) at different content of water in the THF (i.e. anhydrous, HPLC grade, 1 µM, 5 µM, 10 µM or 20 µM) at the beginning of the titration. The binding isotherms are plotted in two scales: (i) whole range and (ii) logarithmic scale. The lines are just interpolations of experimental data.

Characterization of micelles

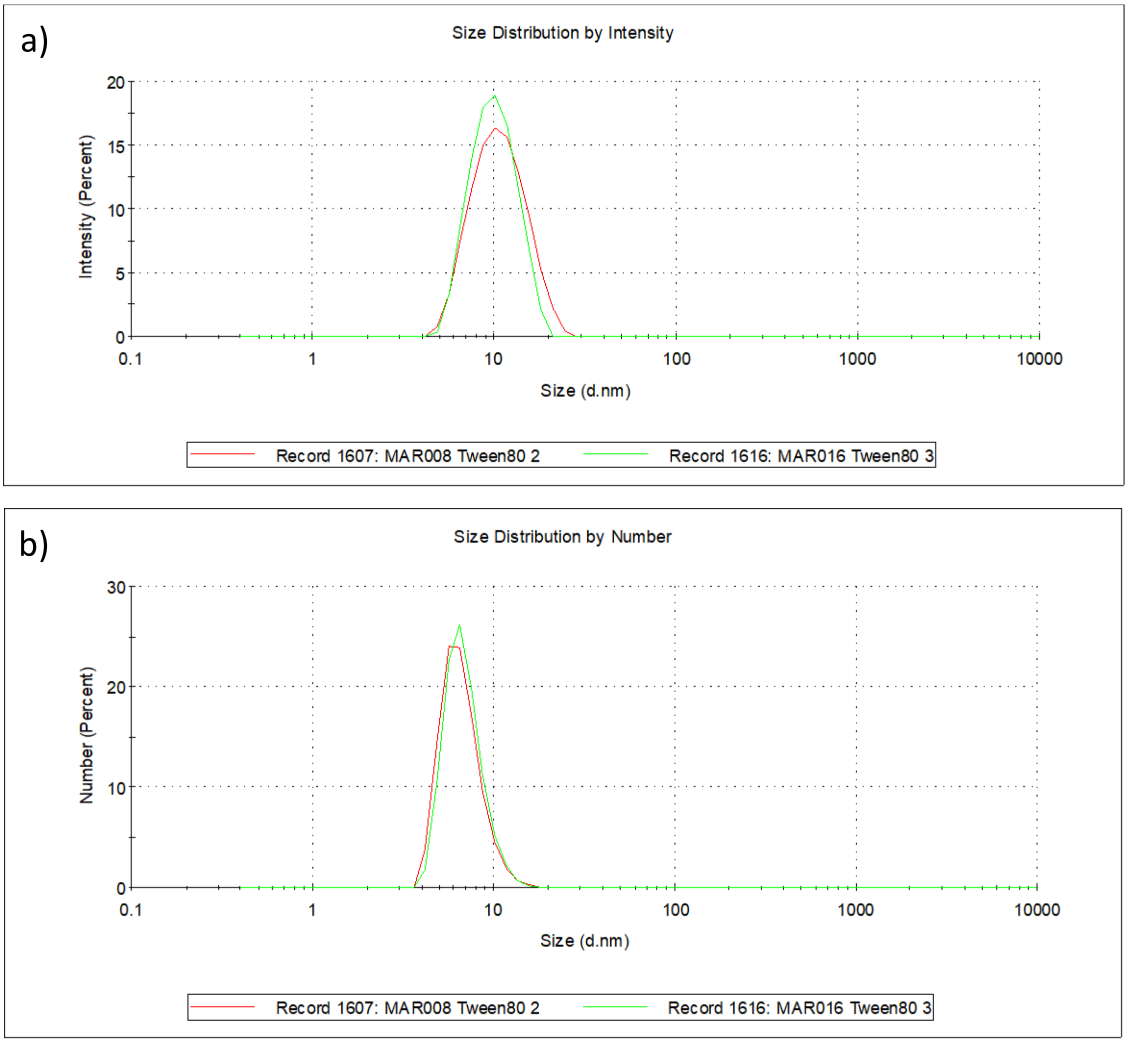

Fig. S18. Size distribution by (a) intensity and by (b) number of micellar solutions of **6c/Tween 80** (green line) and **6d/Tween 80** (red line) in deionized water (pH~6) obtained by dynamic light scattering.

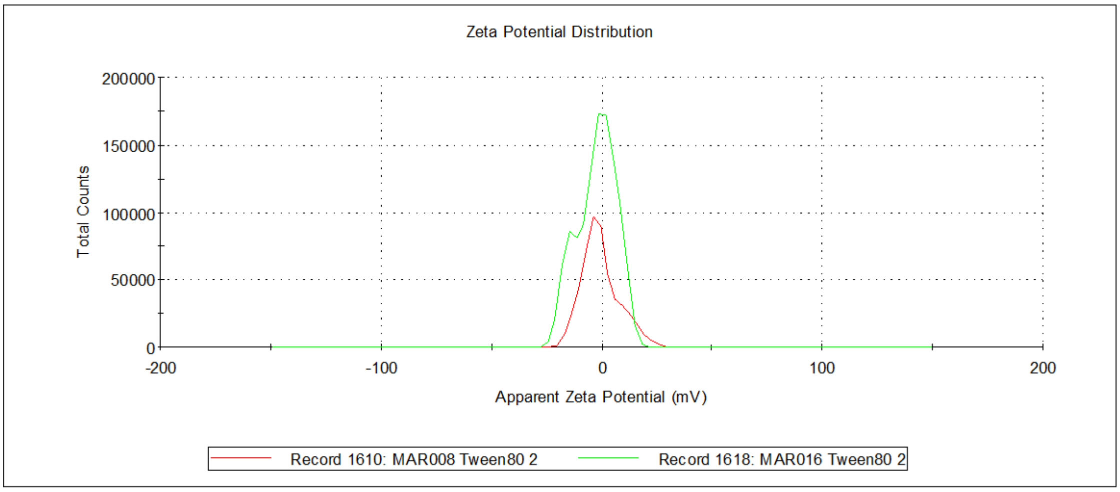

Fig. S19. Zeta potential distribution of micellar solutions of **6c/Tween 80** (green line) and **6d/Tween 80** (red line) in deionized water (pH~6) obtained by dynamic light scattering.

Table S2. Characterization of prepared micelles

Sample	Average size by number [nm]	Hydrodynamic diameter [nm]	Polydispersity index (PDI)	Zeta potential [mV]
6c/Tween 80	6.9 ± 1.7	10.0	0.17	-2.1± 8.7
6d/Tween 80	6.7 ± 1.8	10.0	0.12	-0.6 ± 8.4

Sensing in water

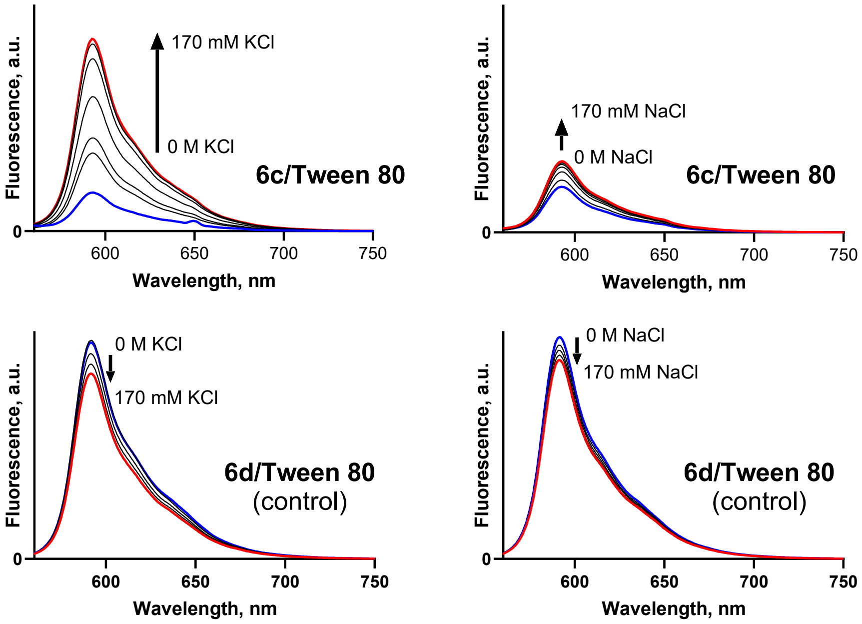

Fig. S20. Changes in fluorescence emission spectra of **6c/Tween 80** and control **6d/Tween 80** upon addition of analyte (KCl or NaCl). Excitation at 530 nm.